

## **Reversible Thermochromism, Temperature-dependent Conductivity and High Stability for a Laminated Bismuth(III)-Silver(I) Hybrid Double Perovskite**

Mohamed Saber Lassoued,<sup>a</sup> Tengbo Wang,<sup>b</sup> Ahmad Faizan,<sup>a</sup> Qian-Wen Li,<sup>a</sup> Wei-Peng Chen<sup>a</sup> and Yan-Zhen Zheng<sup>\*a</sup>

---

[a] School of Chemistry, Frontier Institute of Science and Technology, State Key Laboratory for Mechanical Behavior of Materials, MOE Key Laboratory for Nonequilibrium Synthesis and Modulation of Condensed Matter, Xi'an Key Laboratory of Sustainable Energy and Materials Chemistry, Xi'an Jiaotong University, Xi'an 710049 China.

E-mail : [zheng.yanzhen@xjtu.edu.cn](mailto:zheng.yanzhen@xjtu.edu.cn)

[b] School of Automation Science and Technology, No. 4 Building, Xi'an Jiaotong University, Siyuanhuan North Road, Xi'an, Shaanxi, China.

# Table of content

1. Materials and Sample Preparation.....	3 -
1.1. Materials .....	3 -
1.2. Preparation of $(\text{H}_2\text{MPP})_2[\text{BiAgI}_8]$ Single crystal.....	3 -
2. Characterization methods and Simulation details .....	2 -
2.1. Characterization methods .....	3 -
2.2. Simulation details Computational methods .....	6 -
3. Supporting Tables and Figures .....	8 -
4. References .....	21 -

## **1. Materials and Sample Preparation**

### **1.1. Materials**

Chemicals listed were used as purchased and without further purification: (i) 1-methylpiperidin-4-amine (MPA), 97%, sigma Aldrich; (ii) Bismuth oxide, 9.995%, sigma Aldrich; (iii) Silver oxide, 99%, sigma Aldrich; (iv) hydroiodic acid, 55% w/w aq. soln., stab with 1.5% hypophosphorous acid, sigma Aldrich.

### **1.2. Preparation of $(\text{H}_2\text{MPP})_2[\text{BiAgI}_8]$**

Single Crystals: A reaction mixture containing 1-methylpiperidine-4-amine (0.228g, 2 mmol) and  $\text{Bi}_2\text{O}_3$  (0.465g, 1 mmol) and  $\text{Ag}_2\text{O}$  (0.231 g, 1 mmol) in 5 mL 55% HI, stirred in the air for 10 minutes before transferred to a 15 mL Teflon-lined auto-clave and heated at 160°C for 6 hrs. The reactants were then cooled to room temperature in a rate of 5°C / h to obtain red-rod -like crystals. (Yield: ca. 60% based on Bi).

Thin Film: Dimethylformamide (DMF, Sigma-Aldrich, 99.8%, anhydrous) was used without further purification. Thin film was prepared on indium doped tin oxide (ITO) coated glass substrates. The substrates were cleaned thoroughly and sequentially with commercial detergent in soapy water, deionized water, KOH solution, and in a sonication bath. The substrate was then treated by UV-ozone treatment for 20 min prior before use. Thereafter, the synthesized bimetallic hybrid double perovskite was deposited by spin-coating (speed = 1000 rpm, time = 20s) from DMF solution of  $(\text{H}_2\text{MPP})_2[\text{BiAgI}_8]$  powders. The fabricated film was then annealed at 70 °C for 10 min.

## **2. Characterization methods and Simulation details**

### **2.1. Characterization methods**

#### **X-ray Crystallographic Study**

Single crystal X-ray diffraction (SCXRD) was performed on Bruker SMART APEX II CCD diffractometer by using Mo, ( $\lambda=0.71073 \text{ \AA}$ ) at different temperatures. Intensity data acquisition, data reduction and cell refinement were performed using the “multi-scan” program. The structures were solved by direct methods and

refined with a full-matrix least-squares technique within the SHELXTL program package. <sup>[S1]</sup> The crystallographic details are provided in Tables S1-S4. Crystallographic data for the structural analyses has been deposited at the Inorganic Crystal Structure Database. CCDC number of 2190851 contain the crystal data at the temperature 150 K. The crystallographic data for above compounds can be found in the Supporting Information or can be obtained free of charge from the Inorganic Crystal Structure Database via [http://www.ccdc.cam.ac.uk/data\\_request/cif](http://www.ccdc.cam.ac.uk/data_request/cif).

**Powder X-ray diffraction (PXRD)** for  $(\text{H}_2\text{MPP})_2[\text{BiAgI}_8]$  was performed on a Bruker D8 ADVANCE X-ray diffractometer at different temperatures (298 K, 350 K, 400 K and 450 K). The diffraction patterns were collected in the  $2\theta$  range of  $5^\circ$ – $50^\circ$  with a step size of  $5^\circ/\text{min}$ . The experimental film XRD patterns obtained at room temperature, and simulated powder XRD pattern was acquired by the software of Mercury 2021.1.0.

**Optical absorption measurement.** The UV-vis-NIR diffuse reflection data were obtained at different temperatures and scan wavelength is between 300 nm and 900 nm on a SHIMADZU UV-3600 UV-Vis-NIR spectrophotometer using  $\text{BaSO}_4$  powder as the reflectance reference. The absorption spectra were calculated from reflectance spectra by the Kubelka-Munk function:  $F(R) = \alpha/S = (1-R)^2/2R$ , where R is the reflectance, K is the absorption, and S is the scattering. <sup>[S2]</sup>

**Raman Spectroscopy:** Raman measurements were performed using a Laser Raman Spectrometer (HORIBA) between  $50 \text{ cm}^{-1}$  and  $300 \text{ cm}^{-1}$  at different temperatures. The excitation light source was a 532 nm laser with a power below 1 mW to avoid sample damage.

**Stability studies.** Freshly prepared Perovskites film of  $(\text{H}_2\text{MPP})_2[\text{BiAgI}_8]$  was deposited on clear plate glasses and thereafter they were placed inside sealed jar containing a saturated solution of  $\text{Mg}(\text{NO}_3)_2 \cdot 6\text{H}_2\text{O}$ , stored either in the dark to minimize light exposure and the relative humidity was maintained at  $\sim 55\%$  humidity. <sup>[S3]</sup> The film was not in direct contact with the solution and was analyzed

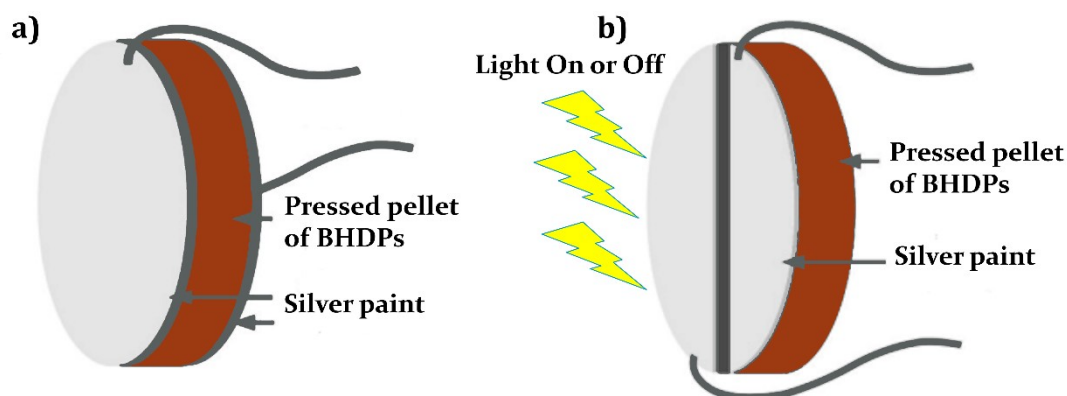
with PXRD after 30 days.

**Photocurrent measurements.** The pellets were prepared by grinding 50 mg polycrystalline sample of  $(\text{H}_2\text{MPP})_2[\text{BiAgI}_8]$  into a homogeneous powder after pressed with 15 MPa for 5 minutes. The pellet was connected to two wires at one side (up or down) using conductive silver paste. It's worthy noting that we left one narrow strip like area without paint which can receive light from the lamp. A 350 W solar-simulating Xenon lamp was used as light source. The devices were placed on a hot plate to achieve a temperature-varying photocurrent test. For each 60 s we past or blocked the light and detected the current change (Scheme 1a).

**Electrical conductivity.** 50 mg powder of  $(\text{H}_2\text{MPP})_2[\text{BiAgI}_8]$  was used to press pellet ( $\phi = 10$  mm) with the thickness about 0.3 mm. Silver conductive paint (SPI supplies co.) was used to stick the wire and the pellet. To test the conductivity under different temperatures, we used an oven to control the temperature. Here, we connect the positive and negative poles to the upper and lower surfaces of the pellets, like the Scheme 1b. We used a source meter (Keithley 2400) serving as a voltage source, and in series with a picoammeter (Keithley 6485) to detect the small currents. The electrical conductivity is calculated by the plots of current density versus electric field strength (J-E curves) based on the following Ohm's law:

$$\sigma = J / E, J = I / S, E = V / L$$

where  $\sigma$  is the conductivity, J is the current density, E is the electric field strength, I is the current, V is the voltage, S is the cross-sectional area of the pressed pellets, and L is the thickness of the pellets.



**Scheme 1** (a) Electrical Conductivity test device. (b) Photo-response test device

**Differential Scanning Microscopy:** The differential scanning calorimetry of  $(\text{H}_2\text{MPP})_2[\text{BiAgI}_8]$  were performed using a DISCOVER DSC250 instrument in the temperature range of 30-550 °C. The crystalline samples were placed in aluminum crucibles that were heated and cooled with a rate of 10 °C /min under the nitrogen atmosphere.

**Thermogravimetric analysis:** Thermogravimetric analyses (TGA) were carried out on a METTLER TOLEDO TGA/DSC3+ Extreme. A heating rate of 10 °C min<sup>-1</sup> under flowing N<sub>2</sub> was used from room temperature to 700°C to investigate the thermal stabilities.

**Scanning Electron Microscopy (SEM):** The morphology of the samples was observed via scanning electron microscopy (Gemini SEM 500). The component analysis of elements was measured by energy-dispersive X-ray spectroscopy (EDS; Esprit Compact).

## 2.2 Simulation details Computational methods.

The crystallographic data of  $(\text{H}_2\text{MPP})_2[\text{BiAgI}_8]$  obtained from Single Crystal XRD tests were used to calculate the electronic band structures and partial densities of the states (PDOS) at 400 K and 450 K. All the calculations in this work were carried out using density functional theory (DFT) as implemented in the BIOVIA Materials Studio Simulation Package. [S4, S5] The generalized gradient approximation (GGA) Perdew–Burke–Ernzerhof (PBE) functional was used for electronic structure calculations. [S6, S7] The convergence threshold for the self-consistent field was  $2 \times$

$10^{-6}$  eV/atom. The pseudopotential form was OTFG ultrasoft mode and the energy cutoff was 489.8 eV. The DFT calculation of  $(\text{H}_2\text{MPP})_2[\text{BiAgI}_8]$  band structure was executed without SOC in an elastic compute servicer with 24 cores and 96 GB memory.

### 3. Supporting Tables and Figures

**Table S1** Crystal data and structure refinement for compound (H<sub>2</sub>MPP)<sub>2</sub>[BiAgI<sub>8</sub>] at different temperatures.

Temperature	150 K	298 K	400 K	450 K	298 K (cooling)
Empirical formula	C <sub>12</sub> H <sub>32</sub> Ag Bi I <sub>8</sub> N <sub>4</sub>	C <sub>12</sub> H <sub>32</sub> Ag Bi I <sub>8</sub> N <sub>4</sub>	C <sub>12</sub> H <sub>32</sub> Ag Bi I <sub>8</sub> N <sub>4</sub>	C <sub>12</sub> H <sub>32</sub> Ag Bi I <sub>8</sub> N <sub>4</sub>	C <sub>12</sub> H <sub>32</sub> Ag Bi I <sub>8</sub> N <sub>4</sub>
Formula weight	1564.47	1564.47	1564.47	1564.47	1564.47
Crystal dimensions (mm)	0.12*0.18*0.14	0.12*0.18*0.14	0.12*0.18*0.14	0.12*0.18*0.14	0.12*0.18*0.14
Crystal system	Monoclinic	Monoclinic	Monoclinic	Monoclinic	Monoclinic
Space group	P2 <sub>1</sub> /n	P2 <sub>1</sub> /n	P2 <sub>1</sub> /n	P2 <sub>1</sub> /n	P2 <sub>1</sub> /n
a/Å	8.505(4)	8.5098(15)	8.5233(18)	8.529(4)	8.502(3)
b/Å	9.833(4)	9.8802(17)	9.950(2)	9.948(5)	9.873(4)
c/Å	19.179(9)	19.225(3)	19.300(4)	19.336(9)	19.221(7)
α/°	90	90	90	90	90
β/°	99.898(4)	99.688(2)	99.419(2)	99.470(5)	99.711(4)
γ/°	90	90	90	90	90
Volume/Å <sup>3</sup>	1580.1 (12)	1593.4(5)	1614.7(6)	1618.2(13)	1590.3(10)
Z	2	2	2	2	2
ρ calcd/cm <sup>3</sup>	3.288	3.261	3.218	3.211	3.267
μ /mm <sup>-1</sup>	14.004	13.887	13.704	13.674	13.914
F(000)	1372.0	1372.0	1372.0	1372.0	1372.0
Index ranges	-10<=h<=10, -12<=k<=12, -24<=l<=24	-10<=h<=10, -12<=k<=12, -24<=l<=24	-10<=h<=10, -12<=k<=12, -24<=l<=24	-10<=h<=10, -12<=k<=12, -24<=l<=24	-10<=h<=10, -12<=k<=12, -24<=l<=24
Data Completeness	99.1%	99.8%	99.7%	99.2%	99.6%
Data/restraints/parameters	3302/0/121	3325/0/121	3344/0/121	3375/0/121	3332/0/121
Goodness-of-fit on F <sup>2</sup>	1.19	1.14	1.13	1.03	1.13
Weight	w = 1/[σ <sup>2</sup> (Fo <sup>2</sup> ) + (0.0156P) <sup>2</sup> + 8.6424P] where P = (Fo <sup>2</sup> + 2Fc <sup>2</sup> )/3	w = 1/[σ <sup>2</sup> (Fo <sup>2</sup> ) + (0.0586P) <sup>2</sup> +18.5591 P] where P = (Fo <sup>2</sup> + 2Fc <sup>2</sup> )/3	w = 1/[σ <sup>2</sup> (Fo <sup>2</sup> ) + (0.0524P) <sup>2</sup> + 5.6108P] where P = (Fo <sup>2</sup> + 2Fc <sup>2</sup> )/3	w = 1/[σ <sup>2</sup> (Fo <sup>2</sup> ) + (0.0415P) <sup>2</sup> + 4.9382P] where P = (Fo <sup>2</sup> + 2Fc <sup>2</sup> )/3	w = 1/[σ <sup>2</sup> (Fo <sup>2</sup> ) + (0.0416P) <sup>2</sup> + 7.6424P] where P = (Fo <sup>2</sup> + 2Fc <sup>2</sup> )/3
R=Σ  Fo-Fc /Σ Fo ,wR <sub>2</sub>	R <sub>1</sub> = 0.025, wR <sub>2</sub> = 0.057	R <sub>1</sub> = 0.05, wR <sub>2</sub> = 0.129	R <sub>1</sub> = 0.042, wR <sub>2</sub> = 0.103	R <sub>1</sub> = 0.034, wR <sub>2</sub> = 0.084	R <sub>1</sub> = 0.046, wR <sub>2</sub> = 0.108

$$R_1 = \frac{\sum ||F_o| - |F_c||}{\sum |F_o|}, wR_2 = \left[ \frac{\sum w(F_o^2 - F_c^2)^2}{\sum w(F_o^2)^2} \right]^{1/2}$$

**Table S2** Summary of selected bond lengths (Å) and bond angles (°) of (H<sub>2</sub>MPP)<sub>2</sub>[BiAgI<sub>8</sub>] at 150 K.

Bond	Lengths/Å	Bond pair	Angles / °	Bond pair	Angles / °
Ag1-I2	3.1472 (12)	I3 <sup>i</sup> -Bi1-I3	174.254 (16)	C1-N1-C6	111.6 (5)
Ag1-I1	2.7100 (12)	I3 <sup>i</sup> -Bi1-I2 <sup>i</sup>	85.837 (11)	N1-C2-C3	111.3 (5)
Ag1-I2 <sup>ii</sup>	3.1472 (12)	I3-Bi1-I2 <sup>i</sup>	90.238 (11)	C5-C5-C4	110.3 (5)
Ag1-I1 <sup>ii</sup>	2.7100 (12)	I3 <sup>i</sup> -Bi1-I2	90.239(11)	N1-C6-C5	110.9 (5)
Bi1-I3	3.0876 (14)	I3-Bi1-I2	85.837 (10)	C2-C3-C4	109.4 (5)
Bi1-I3 <sup>i</sup>	3.0876 (14)	I2-Bi1-I2 <sup>i</sup>	93.89 (4)	N2-C4-C5	109.7 (5)
Bi1-I2	3.1235 (11)	I4-Bi1-I3	91.909 (11)	N2-C4-C3	109.2 (5)
Bi1-I2 <sup>i</sup>	3.1235 (11)	I4-Bi1-I3 <sup>i</sup>	92.277 (11)	C5-C4-C3	111.1 (5)
Bi1-I4	3.0192 (10)	I4 <sup>i</sup> -Bi1-I3	92.275(11)		
Bi1-I4 <sup>i</sup>	3.0192 (10)	I4 <sup>i</sup> -Bi1-I3 <sup>i</sup>	91.911 (11)		
N2-C4	1.513 (7)	I4-Bi1-I2 <sup>i</sup>	89.88 (4)		
N1-C2	1.494 (8)	I4-Bi1-I2	175.613 (11)		
N1-C6	1.500 (7)	I4 <sup>i</sup> -Bi1-I2	89.88 (4)		
N1-C1	1.495 (8)	I4 <sup>i</sup> -Bi1-I2 <sup>i</sup>	175.615 (11)		
C2-C3	1.511 (8)	I4-Bi1-I4 <sup>i</sup>	86.45 (4)		
C5-C6	1.517 (8)	Bi1-I2-Ag1	169.236 (15)		
C5-C4	1.517 (8)	I2-Ag1-I2 <sup>ii</sup>	78.43 (4)		
C3-C4	1.517 (8)	I1 <sup>ii</sup> -Ag1-I2 <sup>ii</sup>	99.30 (2)		
		I1 <sup>ii</sup> -Ag1-I2	103.069 (18)		
		I1-Ag1-I2 <sup>ii</sup>	103.070 (18)		
		I1-Ag1-I2	99.30 (2)		
		I1-Ag1-I1 <sup>ii</sup>	151.02 (4)		
		C2-N1-C6	111.1 (5)		
		C2-N1-C1	112.1 (5)		

Symmetry codes: (i)  $-x+3/2, y, -z+3/2$ ; (ii)  $-x+1/2, y, -z+3/2$ .

**Table S3** Potential hydrogen bonding data of (H<sub>2</sub>MPP)<sub>2</sub>[BiAgI<sub>8</sub>] at 150 K.

D-H	d(D-H)	d(H..A)	<DHA	d(D..A)	A	
N2-H2A	0.89	3.19	134.94	3.871	I2	[-x, -y+1, -z+1]
N2-H2A	0.89	3.025	144.2	3.782	I2	[x-1/2, -y+1, z-1/2]
N2-H2B	0.89	2.893	139.64	3.618	I4	[x-3/2, -y+1, z-1/2]
N2-H2C	0.89	2.812	161.3	3.666	I3	[x-1/2, -y+1, z-1/2]
N1-H1	0.98	2.549	175.12	3.526	I1	
C2-H2D	0.97	3.17	153.35	4.061	I3	[-x+1/2, y, -z+3/2]
C5-H5A	0.97	3.314	142.91	4.13	I1	[-x, -y, -z+1]
C6-H6B	0.97	3.082	132.44	3.804	I3	[-x+1/2, y-1, -z+3/2]
C3-H3B	0.97	3.303	133.15	4.029	I2	[-x, -y+1, -z+1]
C3-H3B	0.97	3.176	137.02	3.942	I1	[-x, -y+1, -z+1]
C4-H4	0.98	3.178	158.47	4.105	I3	[x-3/2, -y+1, z-1/2]

**Table S4.** Selected Silver/Iodide and Bismuth/iodide bond lengths (Å) at different temperatures (150 K, 298 K, 400 K, 450 K and 298 K (after cooling)).

Bond	Bond lengths				
	150 K	298 K	400 K	450 K	298 K (cooling)
Ag1-I2 (Å)	3.1472 (12)	3.1993 (17)	3.2984 (17)	3.3109 (21)	3.1823(16)
Ag1-I1(Å)	2.7100 (13)	2.6981 (8)	2.6752 (9)	2.6767 (14)	2.7054(11)
Ag1-I4 <sup>ii</sup> (Å)	3.7867 (14)	3.7706 (18)	3.7311 (18)	3.7209 (12)	3.7775 (18)
Ag-I (Avg) (Å)	<b>3.2146</b>	<b>3.2226</b>	<b>3.2349</b>	<b>3.2361</b>	<b>3.2217</b>
Bi1-I2 (Å)	3.1235 (11)	3.1166 (8)	3.1047 (8)	3.1033 (12)	3.1188 (10)
Bi1-I3 (Å)	3.0876 (14)	3.0881 (8)	3.0917 (8)	3.0962 (15)	3.0899 (12)
Bi1-I4 (Å)	3.0192 (10)	3.0296 (8)	3.0443 (8)	3.0458 (12)	3.0270 (10)
Bi-I (Avg) (Å)	<b>3.0767</b>	<b>3.0781</b>	<b>3.0802</b>	<b>3.0817</b>	<b>3.0785</b>

Avg: Average

Symmetry codes: (ii)  $-x+1/2, y, -z+3/2$ .

To explain the thermochromism in  $(\text{H}_2\text{MPP})_2[\text{BiAgI}_8]$ , we calculated the average of Bi-I and Ag-I distances. We note that  $(\text{Ag-I})_{\text{avg}}$  bond length elongates obviously from 3.2146 Å to 3.2361 Å, while the  $(\text{Bi-I})_{\text{avg}}$  bond length shows less change from 3.0767 Å to 3.0817 Å. Herein, we need to mention that  $(\text{Ag-I})_{\text{avg}}$  and  $(\text{Bi-I})_{\text{avg}}$  almost return to their initial values after cooling down to room temperature (Fig. S9 (a, b)). Fortunately, calculating average bond distances at different temperatures are well fit with our data and easily to reflect the thermochromism behavior in  $(\text{H}_2\text{MPP})_2[\text{BiAgI}_8]$  (Figures 1c and S9 (a, b)).

**Table S5** Thin film band gap energy comparison of  $(\text{H}_2\text{MPP})_2[\text{BiAgI}_8]$  with other reported related crystalline materials.

Compounds	Thin Films band gaps	References
$(\text{C}_4\text{H}_9\text{NH}_3)_2\text{PbBr}_4$	3.06	[S8]
$\text{Gly}_2\text{PbI}_4$	2.9	[S9]
$(\text{C}_4\text{H}_9\text{NH}_3)_2\text{PbI}_4$	2.4	[S8]
$(\text{MA})_3\text{Bi}_2\text{I}_9$	2.24	[S10]
$(\text{C}_6\text{H}_{16}\text{N}_2)_2\text{AgBiI}_8 \cdot \text{H}_2\text{O}$	2.15	[S11]
$\text{Cs}_3\text{Sb}_2\text{I}_9$	2.05	[S12]
$(\text{C}_6\text{H}_{16}\text{N}_2)_2\text{CuBiI}_8 \cdot 0.5\text{H}_2\text{O}$	2.02	[S11]
$(\text{H}_2\text{MPP})_2[\text{BiAgI}_8]$	1.96	This work

**Table S6.** Stability tests comparison of  $(\text{H}_2\text{MPP})_2[\text{BiAgI}_8]$  with other reported Pb-free halide perovskite materials.

<b>Compounds</b>	<b>Test period (d)</b>	<b>Test condition</b>	<b>Stability</b>	<b>Ref</b>
$(\text{H}_2\text{MPP})_2[\text{BiAgI}_8]$	30	55% RH	Stable	This work
$\text{Cs}_3\text{Bi}_2\text{I}_9$	30	<10% RH	Stable	[S13]
$\text{AgBi}_2\text{I}_7$	10	/	Stable	[S14]
$\text{MA}_3\text{Bi}_2\text{I}_9$	25	61% RH	Stable	[S15]
$\text{C}_5\text{H}_6\text{NBiI}_4$	7	/	Stable	[S16]
$\text{Cs}_2\text{NaBiI}_6$	150	70% RH	Stable	[S17]
$(\text{C}_6\text{H}_{16}\text{N}_2)_2\text{BiAgI}_8 \cdot \text{H}_2\text{O}$	30	55% RH	Stable	[S11]
$(\text{C}_{10}\text{H}_{26}\text{N}_4)_2\text{BiAgI}_8 \cdot \text{H}_2\text{O}$	30	55% RH	Stable	[S18]
$(\text{H}_2\text{EPZ})_2\text{BiAgBr}_8$	90	55% RH	Stable	[S19]
$(\text{H}_2\text{MPA})_2\text{BiAgBr}_8$	90	55% RH	Stable	[S19]

Where MA: Methylammonium/  $\text{H}_2\text{EPZ}$ : 1-ethylpiperazinium/  $\text{H}_2\text{MPA}$ : 1-methylpiperidinium-4-amine

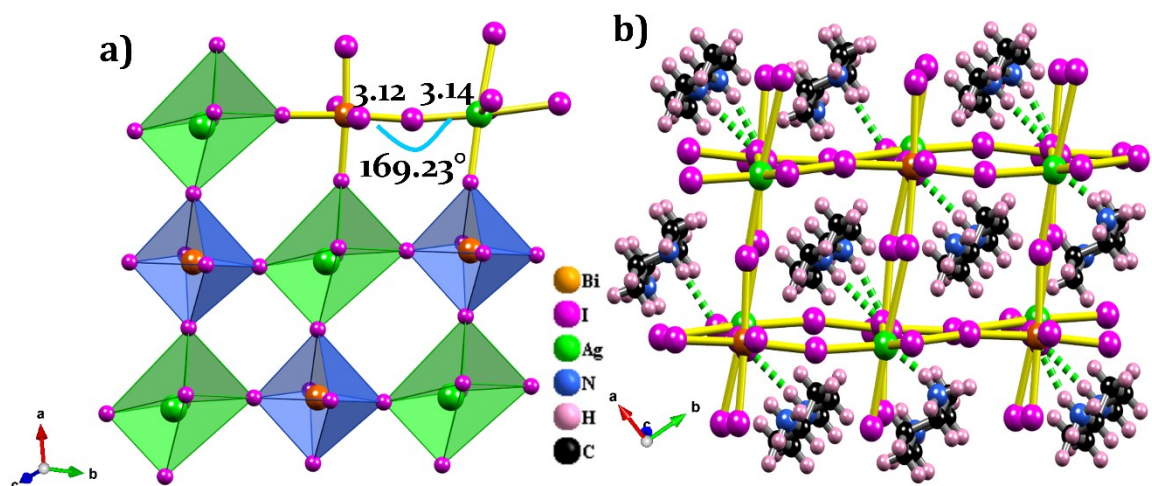


**Figure S1.** (a) Platform of inorganic layers consisting of alternate Ag-I<sub>6</sub> octahedrons and Bi-I<sub>6</sub> octahedrons. (b) The hydrogen bond networks (N-H···I and C-H···I) of (H<sub>2</sub>MPP)<sub>2</sub>[BiAgI<sub>8</sub>] shown in green dashed lines.

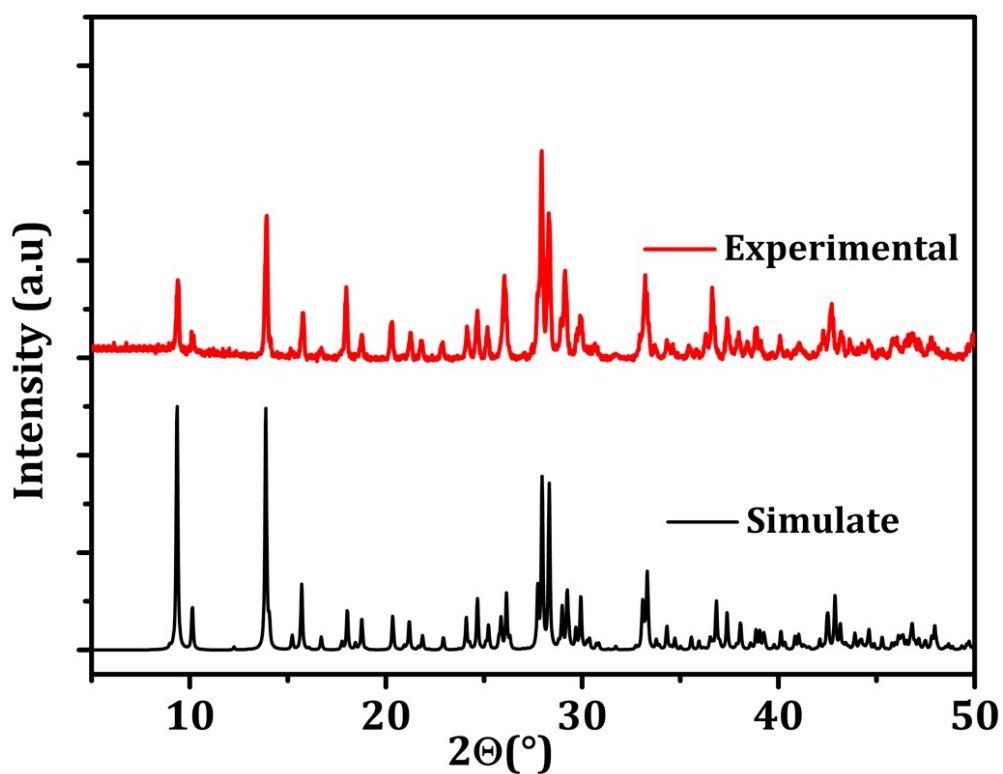


**Figure S2.** Experimental and calculated powder X-ray diffraction (PXRD) patterns of (H<sub>2</sub>MPP)<sub>2</sub>[BiAgI<sub>8</sub>].

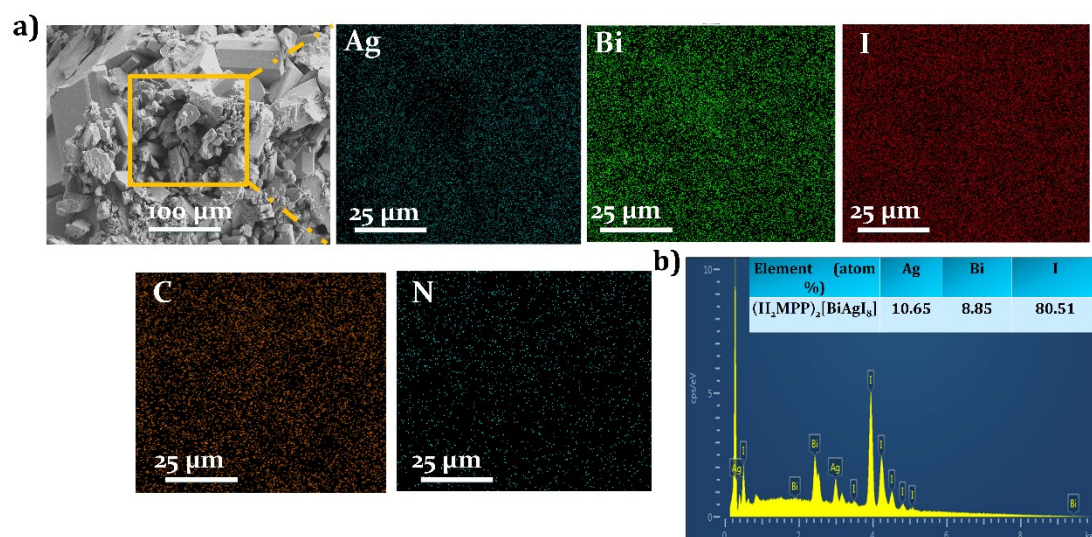


**Figure S3.** (a) SEM and elemental mapping of  $(\text{H}_2\text{MPP})_2[\text{BiAgI}_8]$ . (b) EDS elemental analysis results (Bi/Ag/I) of  $(\text{H}_2\text{MPP})_2[\text{BiAgI}_8]$ .

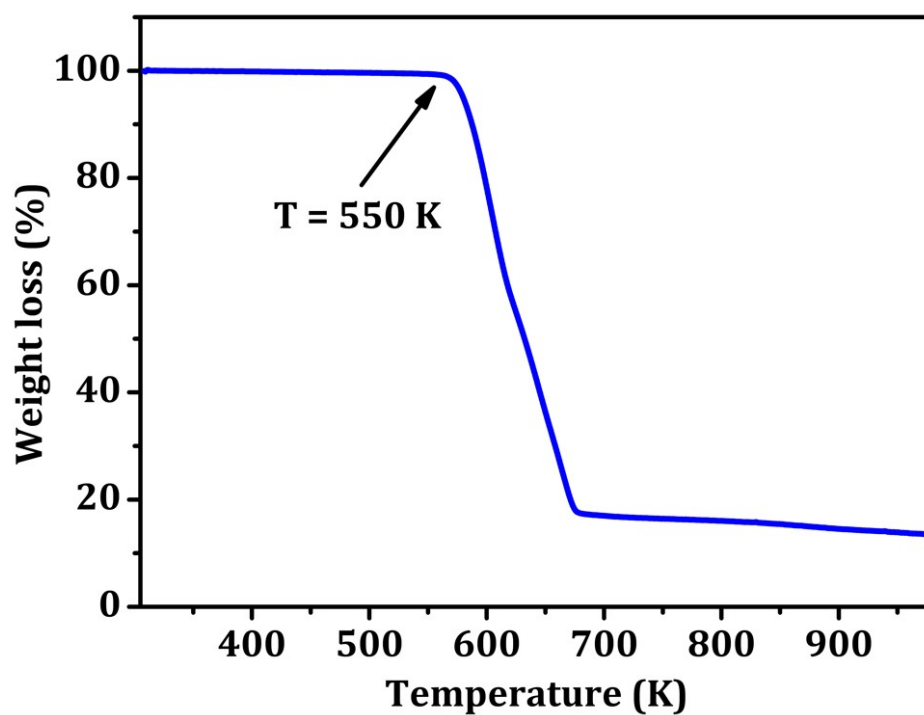


**Figure S4.** Thermal stability of  $(\text{H}_2\text{MPP})_2[\text{BiAgI}_8]$  measured by thermogravimetric analysis (TGA) method under  $\text{N}_2$  atmosphere.

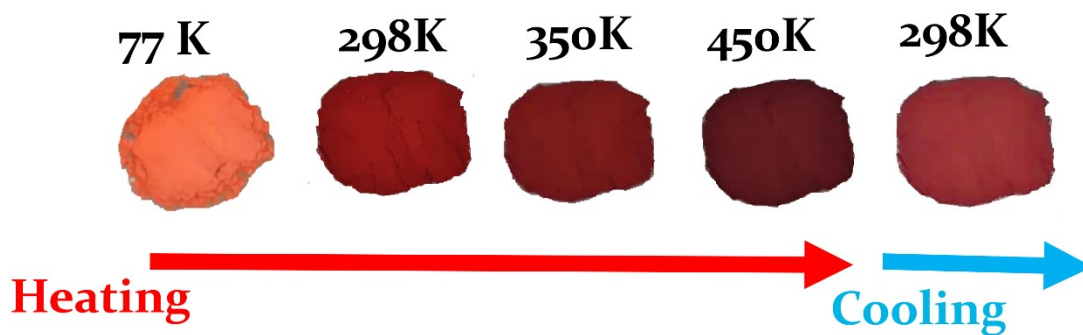


**Figure S5.** Temperature-induced colour change in  $(\text{H}_2\text{MPP})_2[\text{BiAgI}_8]$  powder.

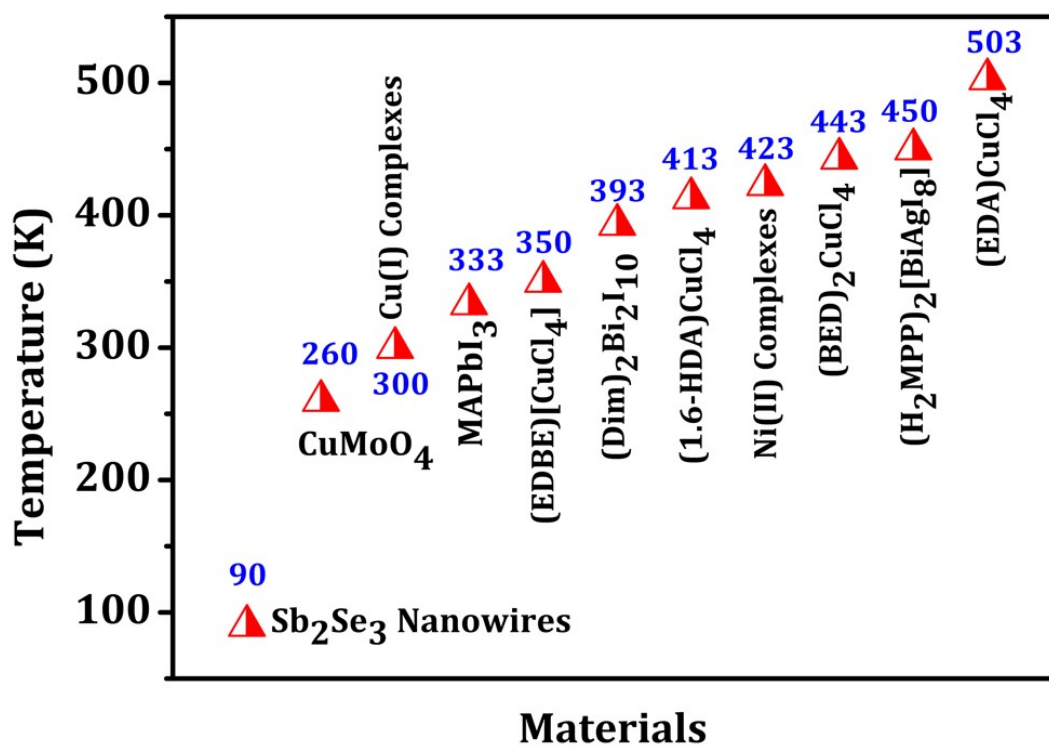


**Figure S6.** Maximum response temperature of thermochromic materials reported in the literature (corresponding to references 20 to 29 from left to right). [S20-S29].

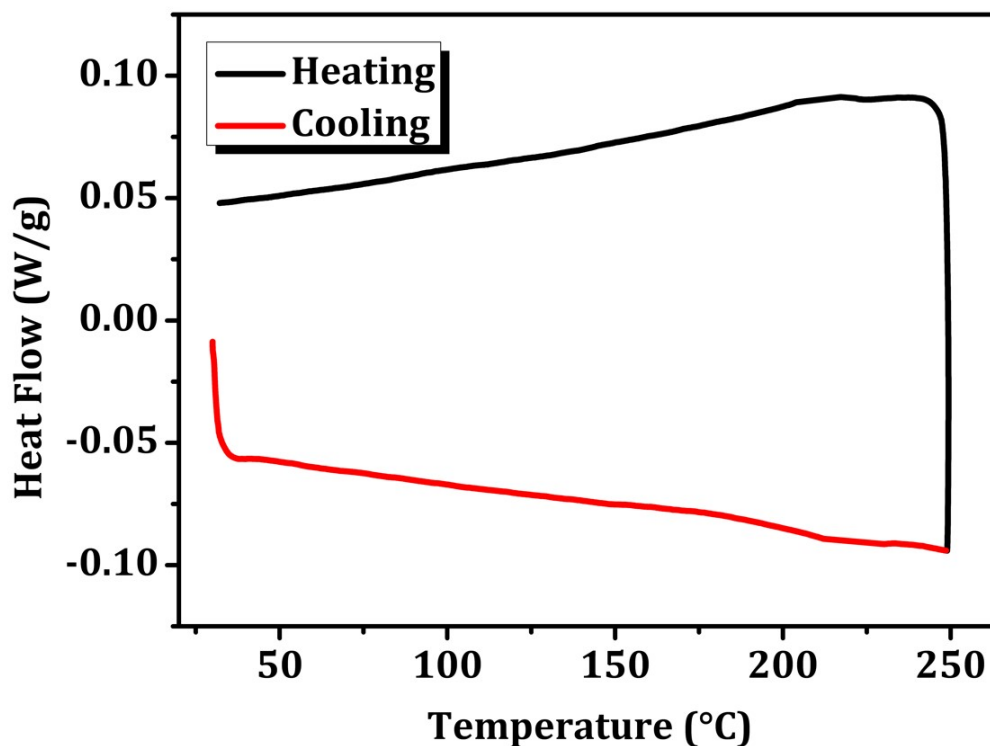


**Figure S7.** Differential scanning calorimetry (DSC) of  $(\text{H}_2\text{MPP})_2[\text{BiAgI}_8]$  with scan rate of 10 K/min under  $\text{N}_2$  atmosphere.

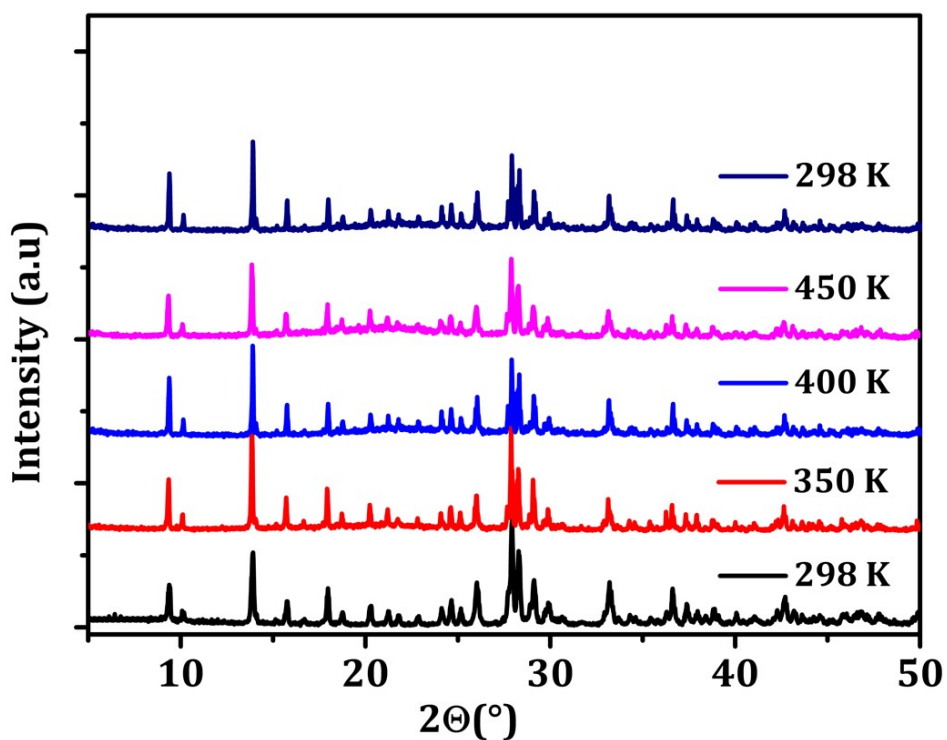


**Figure S8.** XRD diffractograms of  $(\text{H}_2\text{MPP})_2[\text{BiAgI}_8]$  at various temperatures when heating from 298 K to 450 K and cooling back to 298 K (bottom to top).

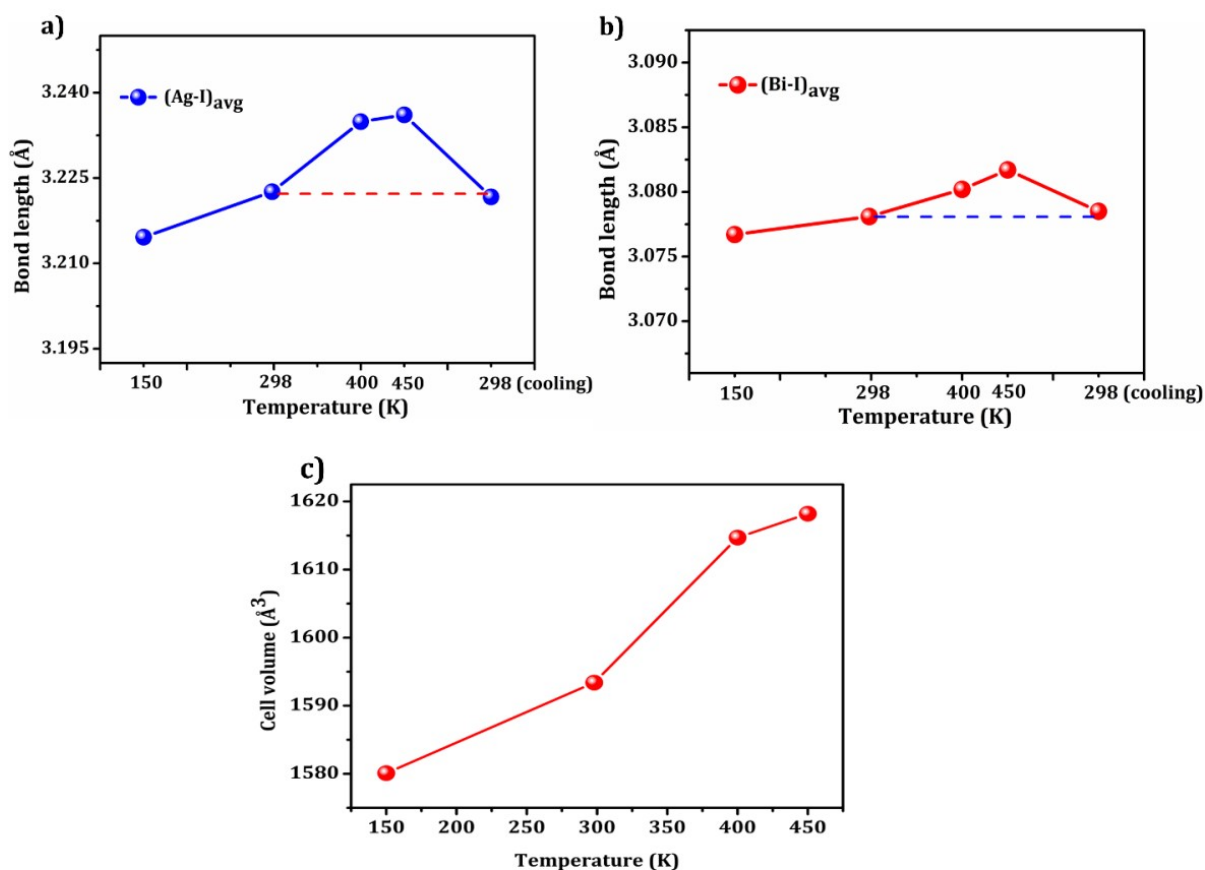


**Figure S9.** (a, b) Variation of  $(\text{Ag-I})_{\text{avg}}$  (a) and  $(\text{Bi-I})_{\text{avg}}$  (b) bond lengths measured at 150 K, 298 K, 400 K, 450 K and 298 K (cooling from 450 K). (c) Temperature-dependent cell volume.

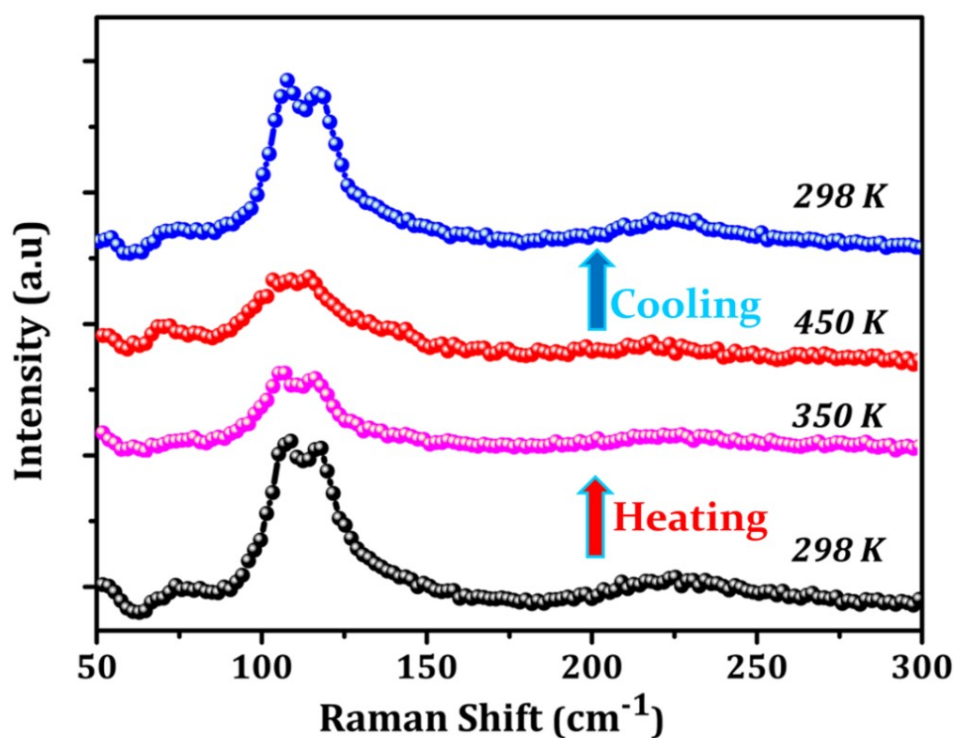


**Figure S10.** Raman spectra of  $(\text{H}_2\text{MPP})_2[\text{BiAgI}_8]$  collected at different temperatures.

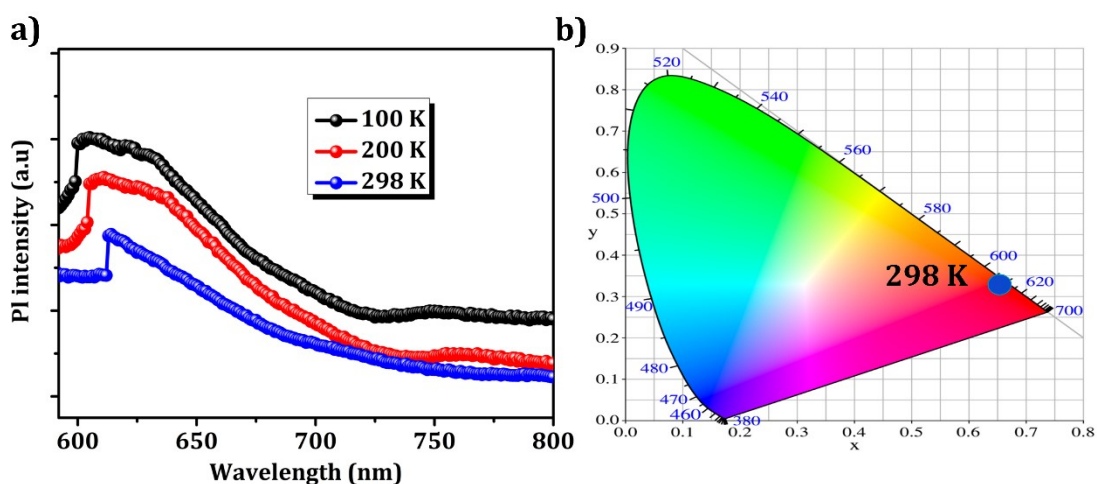


**Figure S11.** (a) PL spectra for the hybrid double perovskite structure  $(\text{H}_2\text{MPP})_2[\text{BiAgI}_8]$  measured at 100 K, 200 K and at 298 K. (b) CIE coordinates of  $(\text{H}_2\text{MPP})_2[\text{BiAgI}_8]$  at 298 K.

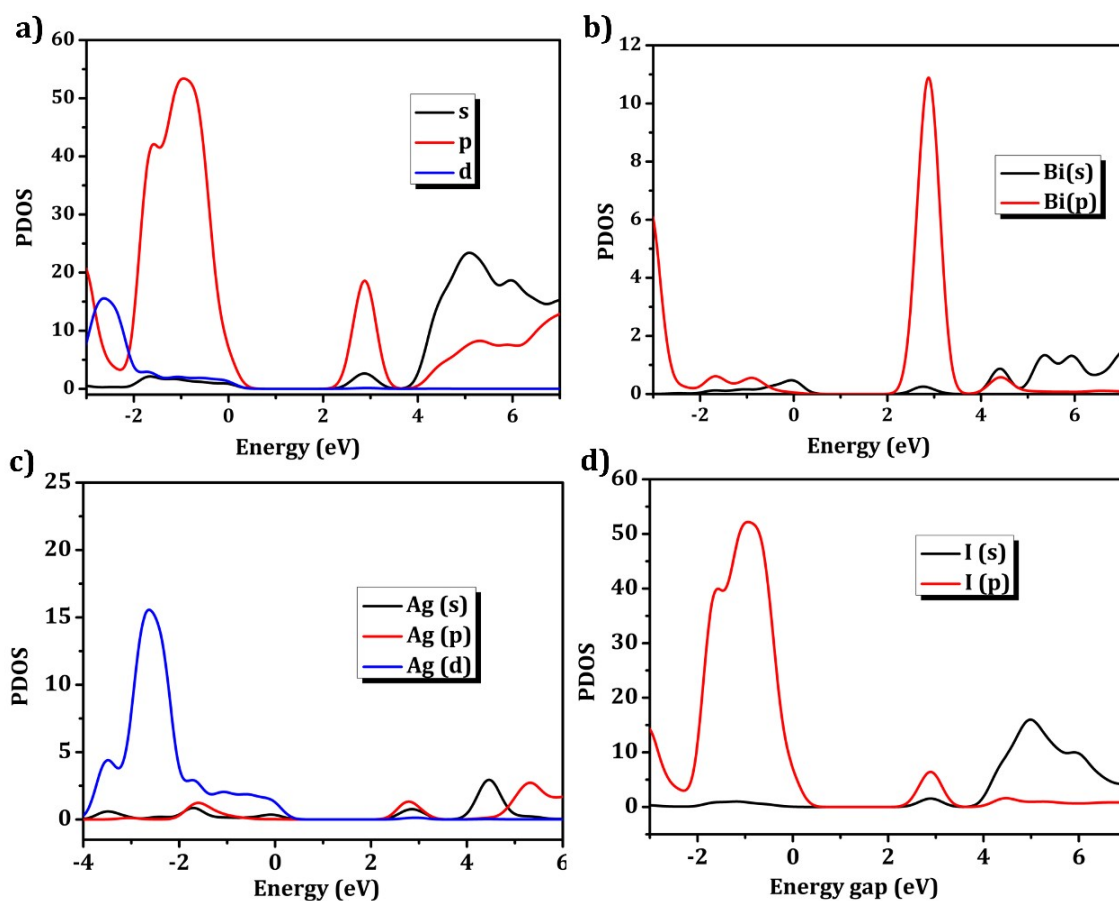


**Figure S12.** Partial density of states (PDOS) (Inorganic part (a), Bi-s and Bi-p (b), Ag-s, Ag-p and Ag-d (c) and I-s, I-p (d)) at 400 K.

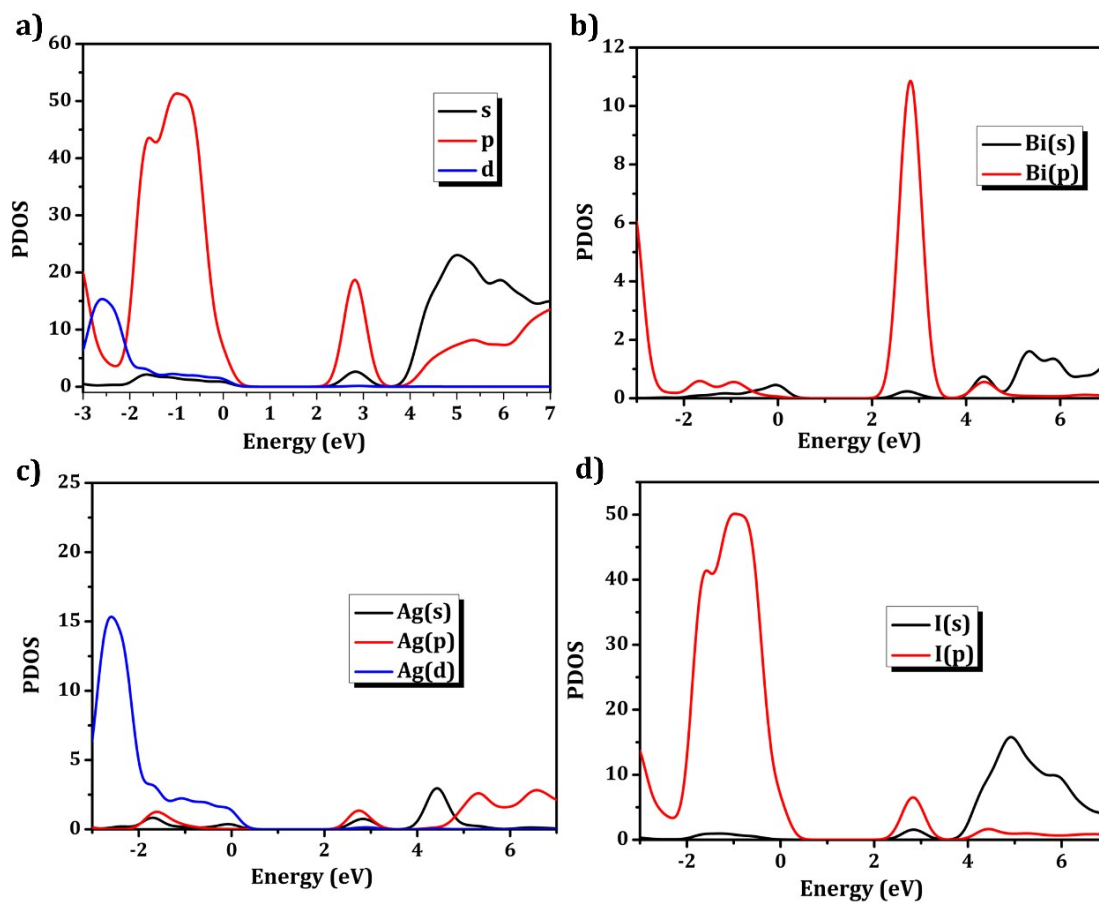


**Figure S13.** Partial density of states (PDOS) (Inorganic part (a), Bi-s and Bi-p (b), Ag-s, Ag-p and Ag-d (c) and I-s, I-p (d)) at 450 K.

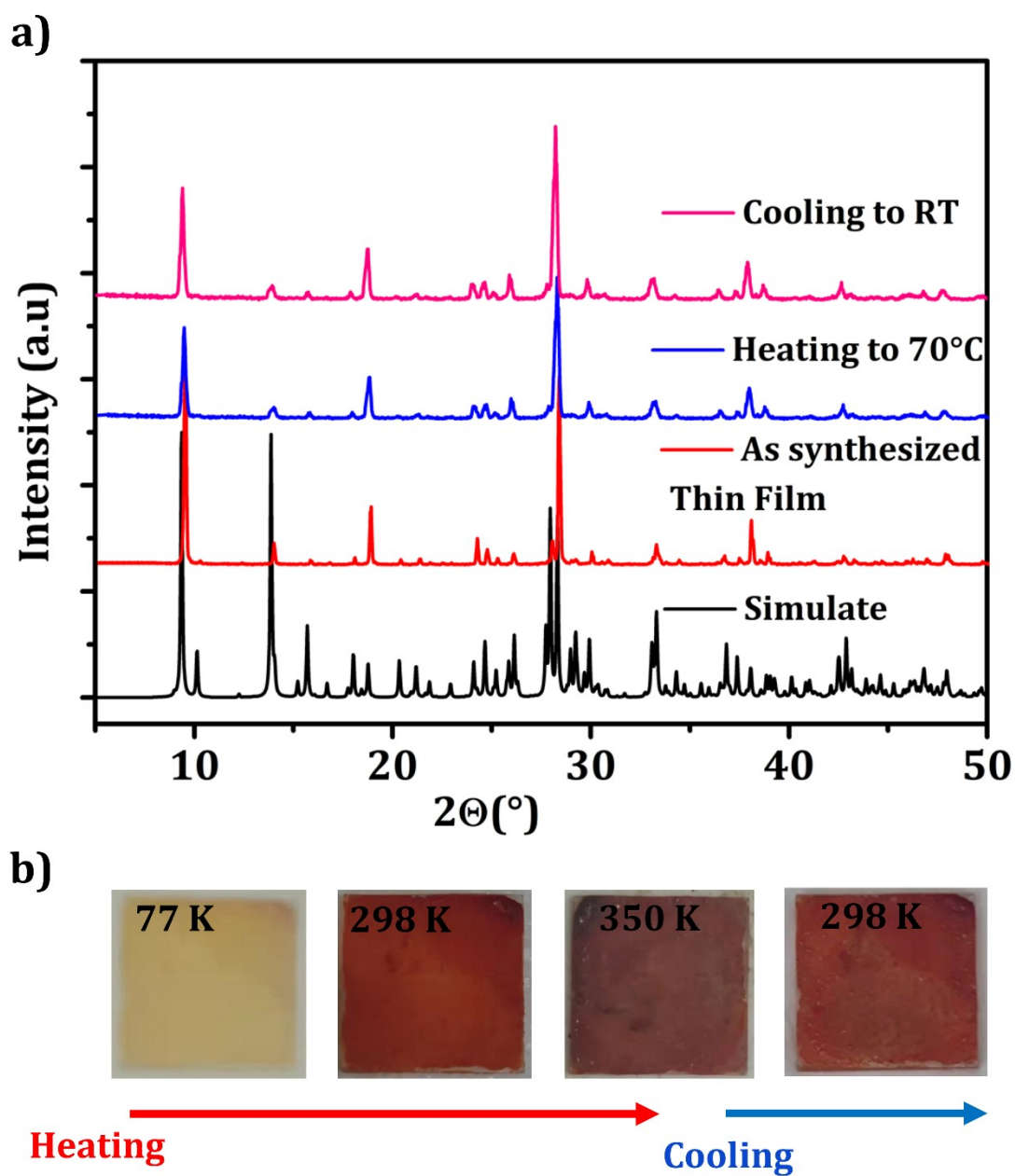


**Figure S14.** (a) XRD patterns of the thin film made from  $(\text{H}_2\text{MPP})_2[\text{BiAgI}_8]$ . (b) Optical images of  $(\text{H}_2\text{MPP})_2[\text{BiAgI}_8]$  thin film at different temperatures.

## References

- [S1] Sheldrick G. A Short History of Shelx [J]. *Acta Crystallographica Section A*. **2008**, *64(1)*, 112-122.
- [S2] Tauc. Absorption edge and internal electric fields in amorphous semiconductors. *J. Mater. Res. Bull.* **1970**, *5*, 721.
- [S3] F. E. M. O'BRIEN, The Control of Humidity by Saturated Salt Solutions, *J. Sci. Instrum.* **1948**, *25*, 73–76.
- [S4] J. Hafner, *J. Comput. Chem.* **2008**. *29*, 2044-2078.
- [S5] Perdew J P, Burke K, Ernzerhof M. Generalized Gradient Approximation Made Simple [J]. *Physical Review Letter.* **1996**, *77(18)*, 3865-3868.
- [S6] D. M. Ceperley and B. J. Alder, Ground-state of the electron-gas by a stochastic method. *Phys. Rev. Lett.* **1980**, *45*, 566.
- [S7] J. P. Perdew and A. Zunger, *Phys. Rev. B: Condens. Matter Mater. Phys.* **1981**, *23*, 5048
- [S8] K. Y. Shi, L. L. Guo, H. X. Liu, L. Zou, S. F. Ying, *Solid State Phenomena*, **2006**, *111*, 119-122.
- [S9] Q. Zhang, J. Zhao, Z. Xiao, J. Zhou, B. Hong, Z. Luo, J. Bao, and C. Gao, *ACS Appl. Energy Mater.* **2018**, *1*, 2502–2511.
- [S10] F. Li, H. Fan, P. Wang, X. Li, Y. Song, and K-J. Jiang, *J Mater Sci.* **2019**, *54*, 10371–10378.
- [S11] L-Y. Bi, Y-Q. Hu, M-Q. Li, T-L. Hu, H-L. Zhang, X-T. Yin, W-X. Que, M. S. Lassoued and Y-Z. Zheng, *J. Mater. Chem. A*. **2019**, *7*, 19662-19667.
- [S12] B. Saporov, F. Hong, J-P. Sun, H-S. Duan, W. Meng, S. Cameron, I. G. Hill, Y. Yan, and D. B. Mitzi, *Chem. Mater.* **2015**, *27*, 5622–5632.
- [S13] B. W. Park, B. Philippe, X. Zhang, H. Rensmo, G. Boschloo and E. M. Johansson, *Adv. Mater.* **2015**, *27*, 6806–6813
- [S14] Y. Kim, Z. Yang, A. Jain, O. Voznyy, G. H. Kim, M. Liu, L. N. Quan, F. P. Garcia de Arquer, R. Comin, J. Z. Fan and E. H. Sargent, *Angew. Chem. Int. Ed.* **2016**, *55*, 9586–9590.
- [S15] R. L. Hoye, R. E. Brandt, A. Osherov, V. Stevanovic, S. D. Stranks, M. W. Wilson,

- H. Kim, A. J. Akey, J. D. Perkins, R. C. Kurchin, J. R. Poindexter, E. N. Wang, M. G. Bawendi, V. Bulovic and T. Buonassisi, *Chem. Eur. J.* **2016**, *22*, 2605-
- [S16] T. Li, Y. Hu, C. A. Morrison, W. Wu, H. Han and N. Robertson, *Sustainable Energy Fuels*. **2017**, *1*, 308–316.
- [S17] C. Zhang, L. Gao, S. Teo, Z. Guo, Z. Xu, S. Zhao and T. Ma, *Sustainable Energy & Fuels*. **2018**, *2*, 2419–2428
- [S18] M. S. Lassoued, L.-Y. Bi, Z. Wu, G. Zhou and Y.-Z. Zheng, *J. Mater. Chem. C*. **2020**, *8*, 5349–5354.
- [S19] M. S. Lassoued, T. Wang, Q.-W. Li, X. Liu, W.-P. Chen, B. Jiao, Q.-Y. Yang, Z. Wu, G. Zhou, S. Ding, Z. Zhang and Y.-Z. Zheng, *Mater. Chem. Front.* **2022**, *6*, 2135-2142.
- [S20] W.-Y. Wu, Y. Xu, X. Ong, S. Bhatnagar, Y. Chan, *Adv. Mater.* **2019**, *31*, 1806164.
- [S21] T. Ito, H. Takagi, T. Asano, *Chem. Mater.* **2009**, *21*, 3376-3379.
- [S22] C. M. Brown, V. Carta, M. O. Wolf, *Chem. Mater.* **2018**, *30*, 5786-5795.
- [S23] A. Halder, D. Choudhury, S. Ghosh, A. S. Subbiah, S. K. Sarkar, *J. Phys. Chem. Lett.* **2015**, *6*, 3180-3184.
- [S24] A. Jaffe, Y. Lin, W. L. Mao, and H. I. Karunadasa, *J. Am. Chem. Soc.* **2015**, *137*, 1673–1678.
- [S25] A. G-Fernandez, I. M-Cives, C. P-Iglesias, S. C-García, D. V-García, A. Fernandez, and M. S-Andujar, *Inorg. Chem.* **2018**, *57*, 7655–7664.
- [S26] H. Fu, C. Jiang, C. Luo, H. Lin, H. Peng, *Eur. J. Inorg. Chem.* **2021**, 4984 –4989.
- [S27] J. Pitchaimani, S. Karthikeyan, N. Lakshminarasimhan, S. P. Anthony, D. Moon, and V. Madhu, *ACS Omega*. **2019**, *4*, 13756–13761.
- [S28] B. Sun, X-F. Liu, X-Y. Li, Y. Cao, Z. Yan, L. Fu, N. Tang, Q. Wang, X. Shao, D. Yang, and H-L. Zhang, *Angew. Chem. Int. Ed.* **2020**, *59*, 203 –208.
- [S29] S. Dutta, D. Vishnu S. K, S. Som, R. Chaurasiya, D. K. Patel, K. Moovendaran, C-C. Lin, C-W. Chen, and R. Sankar, *ACS Appl. Electron. Mater.* **2022**, *4*, 521–530.